KeAi
CHINESE ROOTS
GLOBAL IMPACT

Contents lists available at ScienceDirect

Petroleum Science

journal homepage: www.keaipublishing.com/en/journals/petroleum-science



Hydraulic fracturing induced casing deformation and fault activation: from single-well fracturing to well-factory fracturing



Yu-Ting He a,b , Yin-Tong Guo a,b,* , Yun Jiang c , Xin Chang a,b , Yu-Xiang Jing a,b , Ming-Nan Xu a,b , Chun-He Yang a,b

- ^a State Key Laboratory of Geomechanics and Geotechnical Engineering, Institute of Rock and Soil Mechanics, Chinese Academy of Sciences, Wuhan, 430071, Hubei, China
- ^b University of Chinese Academy of Sciences, Beijing, 100049, China
- ^c Research Institute of Petroleum Exploration & Development, Petrochina, Beijing, 100083, China

ARTICLE INFO

Article history: Received 28 February 2025 Received in revised form 20 July 2025 Accepted 21 July 2025 Available online 25 July 2025

Edited by Jia-Jia Fei

Keywords: Hydraulic fracturing Casing deformation Fault reactivation Well-factory Shale gas

ABSTRACT

Hydraulic fracturing-induced casing deformation and fault activation have greatly hindered the safe and efficient development of shale oil and gas resources. In this study, statistical analysis, physical tests, and numerical simulation methods are used to comprehensively analyze hydraulic fracturing-induced fault activation and casing deformation processes. This study is based on the Longmaxi Formation of LZ block, a deep shale gas reservoir in the southwest Sichuan Basin (China), as a geological background. A large amount of field data on fracturing from the LZ Block is counted, and the main influencing factors are analyzed. The main factors of hydraulic fracturing-induced fault slip are (from strong to weak) parameters related to fluid injection volume, parameters related to segments and clusters, and parameters related to injection rate. Combined with physical experiments and numerical simulations, the fault activation law during fracturing has been studied. The degree of casing deformation and fault slip are linearly correlated. For hydraulic fractures to cross faults is very difficult, fault activation and casing deformation can only be mitigated as much as possible. We find that the number of clusters per segment and the injection rate are negatively correlated with the fault slip distance. Reducing the fluid injection volume can mitigate the fault slip distance. Therefore, low injection rates, low fluid volumes, and more clusters per segment are recommended for fracturing in high-risk segments. It is important to note that the scale and risk of fault activation induced by well-factory fracturing is much higher compared to single-well fracturing. In situations with extremely high risk, the injection volume should preferably not exceed 800 m³ to minimize the risk of geological and casing deformation.

© 2025 The Authors. Publishing services by Elsevier B.V. on behalf of KeAi Communications Co. Ltd. This is an open access article under the CC BY license (http://creativecommons.org/licenses/by/4.0/).

1. Introduction

Before the green transition of the energy system is realized, natural gas is an important transition fuel (Papantonis et al., 2025). In the process of carbon neutrality, the demand for natural gas is gradually climbing. There is an urgent need to fill the huge gap between natural gas supply and demand through the development of shale gas (Chen et al., 2020; He et al., 2023). In the commercial development of shale oil and gas resources, hydraulic fracturing is

Peer review under the responsibility of China University of Petroleum (Beijing).

the most important technology (Fu et al., 2024). However, the widespread utilization of hydraulic fracturing involves the risk of inducing earthquakes (Ellsworth, 2013). Stress and pore pressure changes induced by fluid injection are the main cause of induced earthquakes (Moein et al., 2023). Previous studies have shown that the magnitude of fluid injection-induced earthquakes depends on the volume of fluid injected and the size of the fault at critical stress (Schultz et al., 2018; Li et al., 2023). Fortunately, to date, hydraulic fracturing has not caused earthquakes of magnitude larger than 5.7 (Bao and Eaton, 2016; Schultz et al., 2021). It is worth noting that damage to assets in the underground, such as casing deformation (wellbore deformation), often occurs as a result of hydraulic fracturing-induced earthquakes.

In shale gas reservoir development (Southwest China), the probability of casing deformation is more than 40%. When casing

^{*} Corresponding author.

E-mail address: ytguo@whrsm.ac.cn (Y.-T. Guo).

deformation occurs, subsequent fracturing work cannot be carried out normally, which seriously hinders the safe and economic development of shale gas resources (Zhao et al., 2021). Many new fracturing and cementing techniques have been proposed and explored, but the problem of casing deformation remains unresolved (Shen et al., 2024; Yan et al., 2024). It has been shown and pointed out that casing deformation is a shear deformation caused by fault slip (Lei et al., 2024). And the degree of casing deformation is positively correlated with fault slip (Zhang et al., 2021). This means that to mitigate casing deformation, it is necessary to control or avoid fault slip. The main trigger for fault activation and slip is the increase in pore pressure within the fault after fracturing fluid injection (Hui et al., 2021). Moreover, once the fault activation is triggered, the fault will continue to slide even if the injection is stopped immediately (Das and Zoback, 2011). The distribution of microseismic events can assess hydraulic fracturing induced fault activation. Based on microseismic findings, it has been reported that hydraulic fracturing activates faults with (vertical) lengths of about 10-20 m and, in rare cases, over 100 m (Rutqvist et al., 2013). The number of events associated with the fault decreases gradually as the fracturing location moves away from the fault. The cumulative seismic moment is positively correlated with the injected fluid volume (Sun et al., 2024). Reducing the injection rate can effectively mitigate casing deformation and fault slip (Zhang et al., 2020). The activation of faults can be controlled by a novel hydraulic fracture caging method (Madenova et al., 2025; Frash et al., 2025). This method is to deploy multiple production wells around the injection wells like a cage to prevent the faults to be widespread activated by reducing the formation fluid pressure. It seems feasible, but drilling more wells to control fractures is too expensive for shale gas development.

The Sichuan Basin has the largest seismic activity in the world that is associated with hydraulic fracturing of shale gas wells (Schultz et al., 2020), on top of the natural seismicity caused by the complex geological and structural settings of that area (Fig. 1(a) and (b)). Especially in the LZ block, the stress regime is strike-slip and the formation is significantly overpressurized (much higher than hydrostatic pressure). The pressure coefficient of the target reservoir is approximately 2.0. The LZ block mainly develops deep Longmaxi Formation shale gas, as shown in Fig. 1(c). The depth of the target reservoir is about 3800 m. During the fracturing process, fault reactivation and casing deformation problems occur very frequently in the LZ block. To investigate how to mitigate hydraulic fracturing-induced casing deformation and fault activation, we collected data from 79 wells exhibiting fracture-induced casing deformation and a total of 1935 fractures in LZ block. The principal fracturing parameters influencing casing deformation are analyzed using statistical methods. The relationships between hydraulic fracturing and faults, as well as between faults and casing, were examined through physical experiments and numerical simulations, respectively. A field-scale 3D fracture propagation model for hydraulic fracturing is established based on the 3D discrete element method to quantitatively study the activation and slip processes of faults during hydraulic fracturing. Furthermore, the activation and slip behaviors of the faults are investigated under various parameters such as fluid injection rate, fluid injection volume, approach angle of the faults, and fracturing technique. Several field applications (in LZ block) have also been conducted to validate the conclusions of the theoretical study.

2. Methods

2.1. Data analysis methods

To analyze the effect of hydraulic fracturing parameters on casing deformation, statistical analysis methods will be used to analyze fracturing data from the field. There may be some correlation between the different indicators. Therefore, correlation analysis methods need to be used. The formula for calculating the correlation (PCC, Pearson correlation coefficient) between the different indicators is as follows:

$$\gamma_{xy} = \frac{\mathbf{S}_{xy}}{\mathbf{S}_{x}\mathbf{S}_{y}} \tag{1}$$

where, γ_{xy} is the correlation coefficient, \mathbf{S}_{xy} is the covariance, \mathbf{S}_x is the standard deviation of the indicator x, \mathbf{S}_y is the standard deviation of the indicator y. If the value of the correlation between two indicators is greater than 0.5 or below -0.5, they are defined as being strongly correlated. To analyze the degree of influence of different indicators on casing deformation, gray relational analysis (GRA) and entropy weight method (EWM) are used. The dataset needs to be preprocessed before the gray correlation analysis. Make each type of indicator divided by its mean value to eliminate the effect of the dimension. If there are n wells and each well has m indicators. Then, the gray correlation between the influence factor $\mathbf{x}_i (i=1,2,...,n)$ and the casing deformation \mathbf{x}_0 can be calculated by the following equation:

$$\gamma_{i} = \frac{1}{n} \sum_{k=1}^{n} \frac{\min_{i} \left(\min_{k} |\mathbf{x}_{0}(k) - \mathbf{x}_{i}(k)| \right) + \rho \max_{i} \left(\max_{k} |\mathbf{x}_{0}(k) - \mathbf{x}_{i}(k)| \right)}{|\mathbf{x}_{0}(k) - \mathbf{x}_{i}(k)| + \rho \max_{i} \left(\max_{k} |\mathbf{x}_{0}(k) - \mathbf{x}_{i}(k)| \right)}$$
(2)

where, ρ is the resolution factor, here $\rho=0.5$. Before using the entropy weighting method, the samples should be positively normalized to remove the effect of dimension. All samples are denoted as matrix \mathbf{Y}_i (i=1,2,...,n;j=1,2,...,m). Then, the entropy weight of each indicator can be expressed as:

$$\mathbf{W}_{j} = \frac{1 - \mathbf{E}_{j}}{m - \sum \mathbf{E}_{j}} (j = 1, 2, \dots, m)$$
 (3)

Here.

$$\mathbf{E}_{j} = \begin{cases} \ln (n)^{-1} \sum_{i=1}^{n} \mathbf{P}_{ij} \ln \mathbf{P}_{ij} & \mathbf{P}_{ij} \neq 0 \\ 0 & \mathbf{P}_{ij} = 0 \end{cases}$$
(4)

$$\mathbf{P}_{ij} = \frac{\mathbf{Y}_{ij}}{\sum_{i=1}^{n} \mathbf{Y}_{ij}} \tag{5}$$

where, \mathbf{P} is the weight of each data within the indicator, \mathbf{E}_j is the information entropy of indicator j. Considering the importance of different fracturing parameters in the fracturing design process, the most representative parameters among the strongly correlated parameters are selected to analyze their gray correlation and entropy weight.

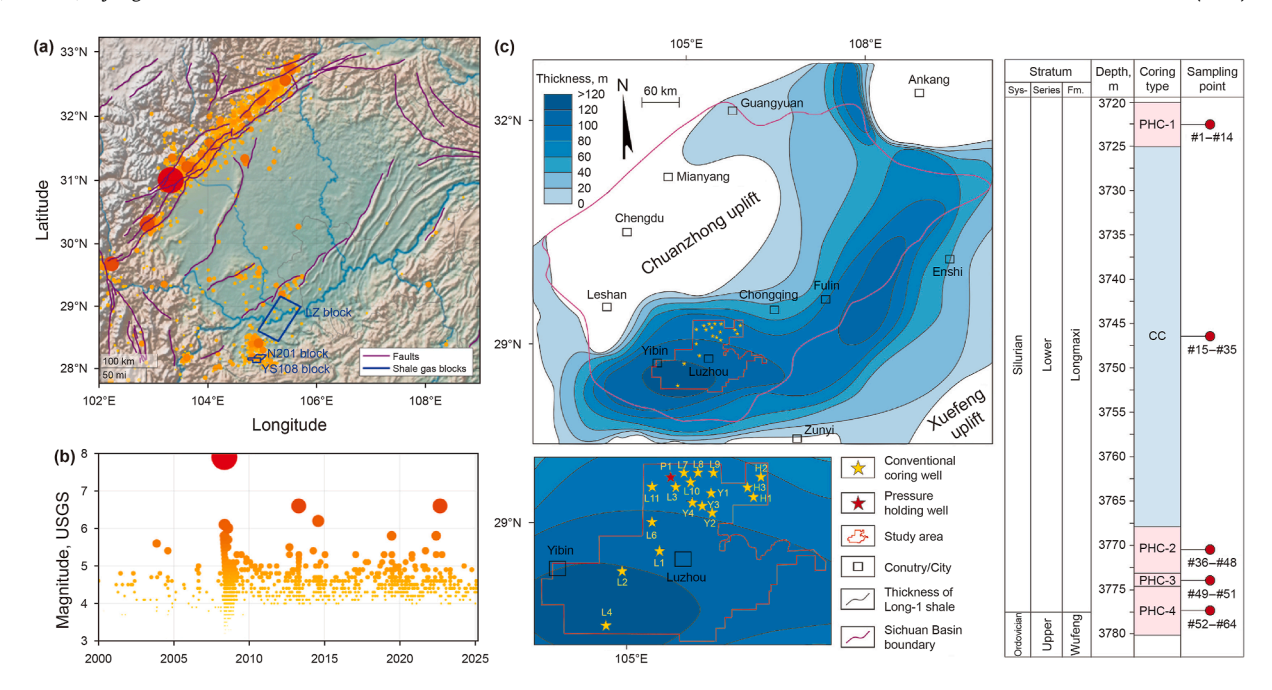


Fig. 1. Geologic background of the LZ block: (a) seismic activity (as reported by the USGS) and active faults (Zelenin et al., 2022) in Sichuan Basin, China, with the location of some shale gas blocks including the LZ block (Xie et al., 2025), and N201 and YS108 blocks (Meng et al., 2019; Tan et al., 2020); (b) seismic activity in the Sichuan Basin of China in recent years; (c) area, reservoir thickness and depth of the LZ block (Li et al., 2024).

2.2. Direct shear test

The test samples are obtained from the shale outcrops of the Longmaxi Formation in Southwest China, which are dark black carbonaceous shales (Zhao et al., 2023; Chang et al., 2024). The test sample for the straight shear test is a rectangular block with dimensions of $50 \times 50 \times 30$ mm. To eliminate the effect of shale laminations on the shear results in the test, the direction of sample laminations is required to be perpendicular to the sheared surface. Half of the sample is soaked by the fracturing fluid in the autoclave until the weight of the sample no longer changes. Direct shear tests at normal corresponding forces of 2.0, 4.0, 6.0, and 8.0 MPa are carried out on the RMT-150C rock mechanics testing system

(Fig. 2(a)), respectively. The horizontal loading rate is 0.6 mm/min. The test is stopped when the peak strength is present. The cohesion and angle of internal friction of the sample can be fitted based on the Mohr-Coulomb criterion.

2.3. Simulation of casing deformation

To study the relationship between fault slip and casing deformation, a numerical model needs to be established, which contains a wellbore and a simplified fault. The linear elasticity constitutive model is adopted and numerically discretized based on the finite element method, as follows (He et al., 2024).

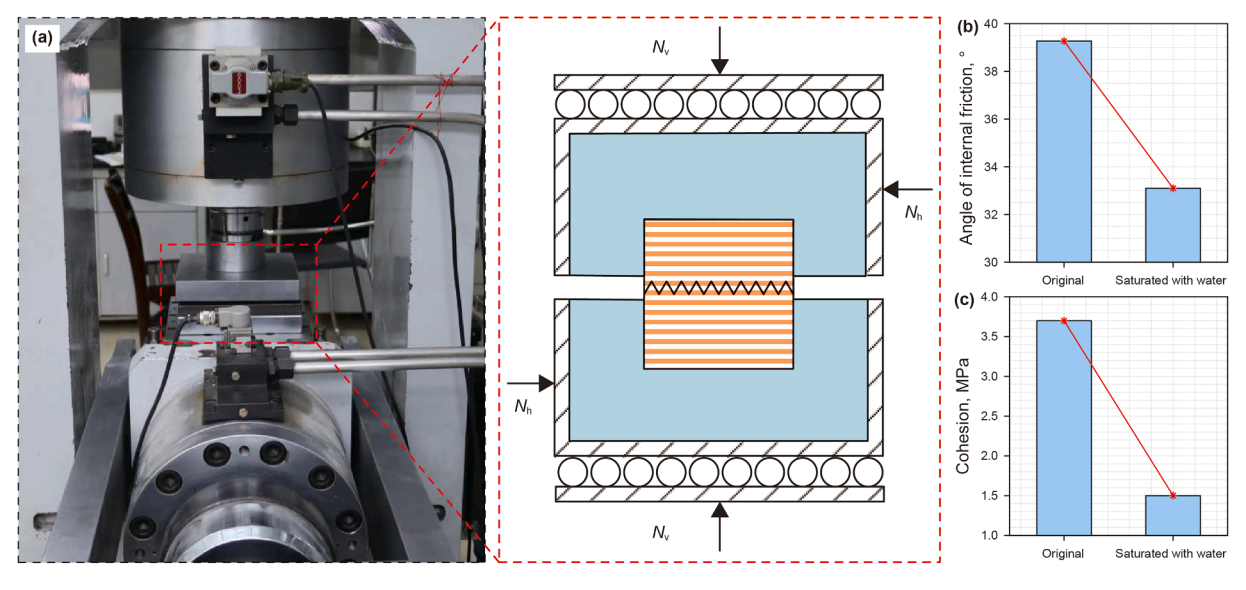


Fig. 2. Direct shear test: (a) the RMT-150C rock mechanics testing systems; (b) the internal friction angle of the weak structural surfaces of the shale; (c) the cohesion of the weak structural surfaces of the shale.

$$\int_{\Omega} \mathbf{B}_{u}^{T} \mathbf{D} \mathbf{B}_{u} \widehat{\mathbf{u}} d\Omega - \int_{\Omega} \mathbf{N}^{T} \mathbf{t} d\Omega = 0$$
 (6)

where, **B** is the geometric matrix, **D** is the matrix of elasticity coefficients, $\hat{\boldsymbol{u}}$ is the node displacement, **N** is the matrix of form function, **t** is the external load on the node. The simulation of interface damage is based on the cohesive damage model, and the B-K criterion is chosen. To eliminate boundary effects, the physical model should have side lengths of the cross-section in the radial direction of the borehole that is more than 10 times larger than the empirical diameter based on Saint Venant's Principle. The size of this cross-section is 3 × 3 m in this study (see Fig. 2(a)). The numerical solution of the model is based on Abaqus.

2.4. Simulation of fault activation

2.4.1. Analytic model

Based on the fracture containing infinitely dimensioned flat plate problem under shear stress in elastodynamics, the analytical solution model for the displacement of a type II fracture can be expressed as follows:

$$u_{\tau} = \frac{4\tau_0}{F'} \sqrt{l_{0.5}^2 - l^2} \tag{7}$$

where, $E' = E/(1-v^2)$, E is Young's modulus, v is Poisson's ratio (see Table 3), τ_0 is shear stress, u_τ is shear displacement, $l_{0.5}$ is half length of the fracture, l is distance from the center of the fracture. Considering the effect of fluid pressure in the fracture, the shear stress on the surface of a closed fracture can be expressed as (Liu et al., 2019):

$$\tau_0 = \tau_{xy} - \mu(\sigma_n - p^*) \tag{8}$$

where, τ_{xy} is the shear stress on the fracture surface by the far-field stresses, μ is the friction coefficient of the fracture surface, σ_n is the normal stress at the fracture surface, p^* is the fluid pressure inside the fracture. Further, the tangential displacement of the closed fracture can be expressed as:

$$u_{\tau} = 4\left(1 - v^{2}\right) \frac{\left[\tau_{xy} - \mu(\sigma_{n} - p^{*})\right]a}{E} \sqrt{{l_{h}}^{2} - l^{2}}$$
(9)

The normal and tangential stresses on the fracture surface induced by far-field stresses can be calculated by the following equation:

$$\begin{split} \sigma_{n} &= \frac{1}{2}(\sigma_{H} + \sigma_{h}) + \frac{1}{2}(\sigma_{H} - \sigma_{h})cos2\beta \\ \tau_{xy} &= \frac{1}{2}(\sigma_{H} - \sigma_{h})sin2\beta \end{split} \tag{10}$$

where, $\sigma_{\rm H}$ is the maximum horizontal principal stress, $\sigma_{\rm h}$ is the minimum horizontal principal stress, β is the approximation angle (the angle between the fault and the direction of the maximum horizontal principal stress).

2.4.2. Numerical model

To study the process of hydraulic fracturing and fault activation, a fracture propagation model is established which considers the hydro-mechanical coupling process. Both the stress field and the flow field are discretized by the finite difference method. The motion equation of each node in the stress field can be expressed as (He et al., 2025):

$$\mathbf{a} = \frac{\int \sigma_{ij} \mathbf{n}_j \mathrm{d}s + \mathbf{F}_i}{m} + \mathbf{g}_i \tag{11}$$

where, **a** is the acceleration of the node, σ is the stress of the node, \mathbf{n}_j is the stress direction vector, m is the mass in the control domain of the node, \mathbf{F} is the external load, \mathbf{g} is the body force. The fluid flow equation can be expressed as:

$$\mathbf{v} = -\frac{k}{\mu_{\rm f}} \nabla p \tag{12}$$

where, k is the permeability, μ_f is the fluid viscosity, p is the fluid pressure. When the fluid flows inside the fracture, the fracture permeability can be expressed as: $k = w^2/12$, w is the fracture width (He et al., 2025). In this study, Mohr-Coulomb law is used to simulate the fracture propagation process. Both shear and tensile fracture processes are integrated into the model. For the unfractured matrix, the tensile normal force is limited to:

$$f_{\text{max}} = -\sigma_{\text{c}} A_{\text{c}} \tag{13}$$

where, σ_c is the tensile strength, A_c is the fracture area. The maximum shear force allowed is:

$$f_{\max}^{s} = CA_{c}\sigma_{n} \tan \phi \tag{14}$$

where, C and ϕ are the cohesion and the internal friction angle. If a fracture occurs, the tensile strength and cohesion are zero, regardless of whether the node is in tension or shear.

3. Results and discussion

3.1. Analysis of casing deformation and fault slip

This study is based on the deep shale gas LZ block in southern Sichuan, China. A total of 1935 fracturing data from 79 wells with fracturing-induced casing deformation are collected and statistically analyzed. All of these wells are located in the LZ block and the horizontal sections are in the Longmaxi Formation. Twenty indicators are selected to investigate the factors that influence casing deformation. The results of the correlation analysis among the indicators are shown in Fig. 3(a). We found that parameters such as proppant/acid injection volume, segment length, and number of clusters are strongly correlated with the total injection volume. This is because the different injection fluids or additives in the fracturing fluid are usually in a fixed ratio to the total injection volume for convenience during fracturing design. Segment or cluster changes can directly affect the total injection volume. Based on GRA and EWN (Sections 2.1), respectively, the degree of influence of different indicators on casing deformation slip is analyzed, and the results are shown in Fig. 3(b) and (c) respectively. The top 30% of influencing factors obtained by GRA are fractured segment length, acid injection volume, injection rate per cluster, proppant injection volume, cluster spacing, injection rate per single perforation hole, and number of clusters per segment. The top 30% of influencing factors obtained by EWN are the number of clusters per segment, segment length, injection rate, cluster injection rate, cluster spacing, injection rate per single perforation hole, and total number of perforation holes. Comprehensively analyzing the results of PCC and the connection between the parameters during fracturing design, we found that the influencing factors are (from strongest to weakest) the parameters related to fluid injection volume, the parameters related to

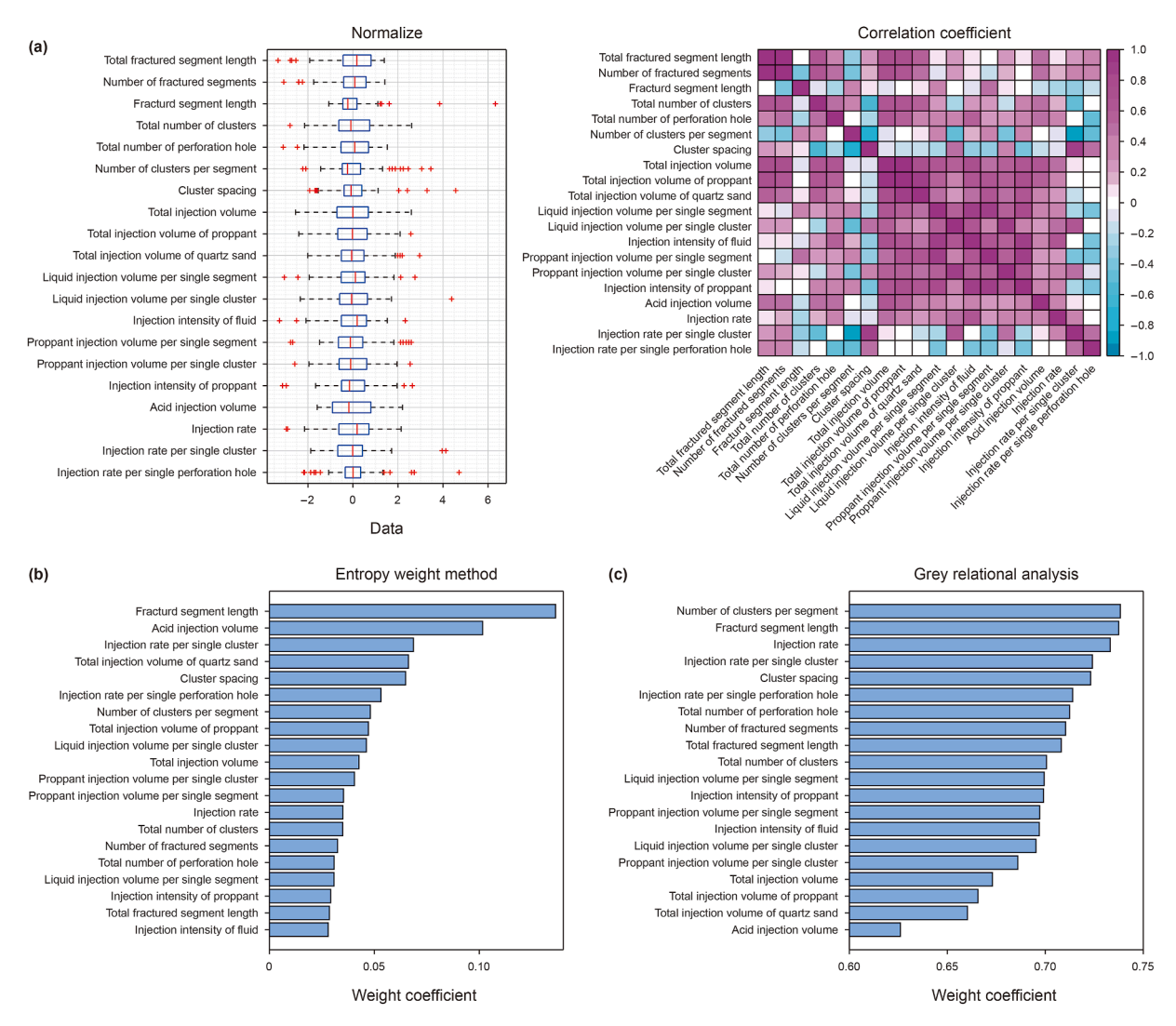


Fig. 3. Results of field data analysis: (a) results of correlation analysis between indicators; (b) results of gray correlation analysis; (c) results of entropy weighting method.

segments and clusters, and the parameters related to injection rate. In addition, recent studies have shown that hydraulic fracturing-induced earthquakes are also associated with larger injection volumes and that the magnitude of earthquakes is linearly related to the fluid injection volume (Schultz et al., 2018).

According to reported studies (Zhang et al., 2021; Lei et al., 2024), fracturing induces fault activation and slip, and fault slip induces casing deformation. To analyze the relationship between fault slip and casing deformation, a geologic model (Fig. 4(a)) containing a fault and a horizontal wellbore is established based

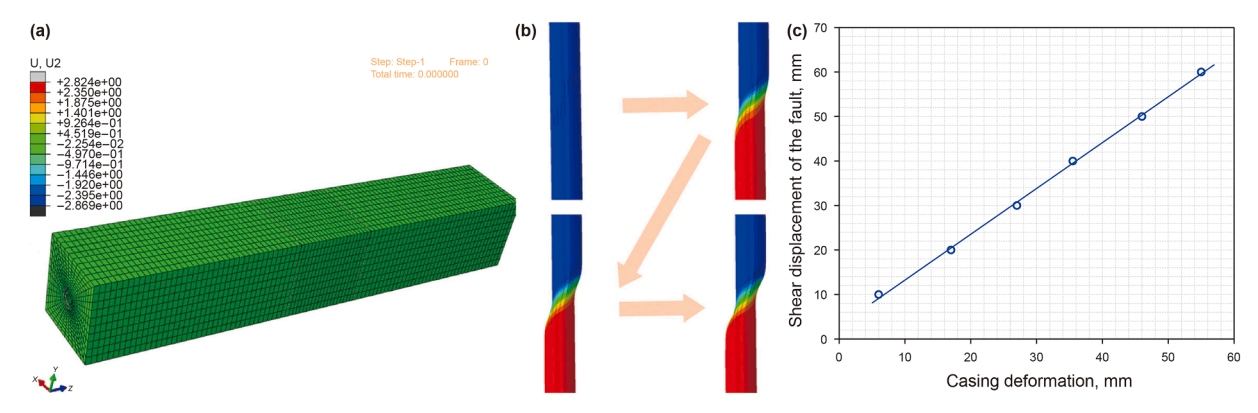


Fig. 4. Numerical simulations and physical experiments on fault activation and casing deformation: (a) the geologic model containing a fault and a horizontal; (b) the casing deformation caused by fault slip; (c) casing deformation under different fault shear displacements.

on the numerical model in Section 2.3. One side of the fault is fixed, and slip is achieved by applying additional loads to the formation on the other side. The input parameters of the model are shown in Tables 1 and 2. The casing deformation caused by fault slip is shown in Fig. 4(b). Statistics of fault slip and casing deformation under different loads (Fig. 4(c)) show that fault slip and casing deformation are linearly correlated (almost identical). The main reason for fault activation is the pore pressure raising caused by fluid injection during the fracturing process. In addition to the effect of fluid pressure, through tests (Section 2.2), we have found that the fracturing fluid entering the fault will cause the cohesion and internal friction angle of the weak structural surfaces of the shale to be reduced (Fig. 2(b) and (c)) (Dou et al., 2020). This will directly make the faults more susceptible to being activated, which will further increase the activation scale of the faults.

3.2. Fault activation and slip induced by hydraulic fracturing

Before studying how to reduce the scale of fault activation induced by hydraulic fracturing, the interaction law between hydraulic fracturing fractures and faults needs to be known. It has been reported that the higher the fluid injection rate per fracture, the easier it is to cross the weak structural surface (Xu et al., 2019; Zheng et al., 2022). Initially, we planned to increase the fluid injection rate per fracture by decreasing the number of clusters and hoped to hydraulic fracture across the fault. Therefore, in the cases with a small number of clusters (four clusters per section), we carried out the study of the interaction law of hydraulic fractures and faults. The numerical model used is shown in Section 2.4.2. The study object is the deep shale gas reservoir of the LZ block in Southwest China, and the input parameters of the numerical model are shown in Table 3. Comparing the lengths of activated faults under different injection rates and approximation angles of the faults (Fig. 5(a)), we found that it is very difficult to cross the faults by the common fracturing techniques. Even if a few individual hydraulic fractures can cross the fault at a large approximation angle, the fractures cannot continue to propagate, and a large amount of fluid will continue to enter the fault. This will probably cause a higher risk of fault activation. On the other hand, we also found that the activation length of a fault is negatively correlated with the approximation angle of the fault. This is because the normal stress on the fracture surface is lower with a smaller approximation angle of the fault, which means that the fault is easier to activate. It is worth noting that the fact that faults are more readily activated does not mean that fault slip distance will increase since the decrease of normal stress may follow the reduction of shear stress. After comparing the fault slip distance under different injection rates and fault angles (Fig. 5(b)), we found that the hydraulic fracturing-induced fault slip distance does not increase monotonically with the decrease of the fault approximation angle. Instead, there is a peak at the approximation angle of the fault close to the internal friction angle of the fault. The slip distance of faults with an approximation angle of 15° is only 44.50%–75.31% of that of faults with an approximation angle of 30°, with an average of 55.71%.

Under specific fault conditions, how to design engineering parameters that can reduce the length and slip distance of activated faults is a major problem for scholars and engineers. Therefore, under maximum risk conditions (the approximation angle of fault is 30°), we compared activated fault lengths and slip distance under different numbers of clusters, injection rates, and volumes of injected fluids (Fig. 6). We find that the slip distance of the activated fault and its length is positively correlated, as shown in the gray zone in Fig. 6(a). In the analytical model (Section 2.4.1), the slip distance of the activated fault is linearly correlated with its length, and the results of the numerical and analytical models have a good concordance. Moreover, the slip distance of the activated fault is positively correlated with the fluid injection volume (Fig. 6 (b)). In the early stage, the maximum shear displacement of the activated faults increases gradually with the increase of the fluid injection volume. In the late stage, the fluid injection volume and the maximum shear displacement of the activated faults are approximately linearly related. This law is consistent with the shear damage process of fluid-injected fractures in the reported study reported by Bhattacharya and Viesca (2019). We found that an injection volume of 1600 m³ can demarcate the early stage and the late stage. When the injection volume is larger than 1600 m³, the slip distance of the fault is linearly related to the injection volume, as shown in the green zone in Fig. 6(b). When the injection volume is less than 1600 m³, it is a nonlinear stage (the red zone in Fig. 6(b)). When the injection volume is less than 1600 m³, increasing the number of clusters per segment can mitigate the fault slip. The fault slip can be mitigated by adopting a lower injection rate. Comparing the relationship between the injection rate per cluster and the fault slip (Fig. 6(c)), we found that the fault slip can also be mitigated by using a lower single-cluster injection rate.

3.3. Wide-scale activation of faults induced by well-factory fracturing

Generally, during the fracturing of shale reservoirs, the fluid volume injected per segment is rarely more than 2000 m³. According to the results in Section 3.2, the maximum fault slip distance is less than 36 mm when the injection volume is 2000 m³,

Table 1Physical model and geologic parameters for fault slip and casing deformation simulation.

Parameters	Value	Unit	Parameters	Value	Unit
Casing inner diameter	139.7	mm	Maximum horizontal principal stress	82.0	MPa
Casing thickness	12.7	mm	Minimum horizontal principal stress	55.0	MPa
Borehole diameter	215.9	mm	Stress gradient	0.023	MPa/m
Overburden stress	50.6	MPa	Casing internal pressure	75.0	MPa

 Table 2

 Material parameters for the simulation of fault slip and casing deformation.

Material	Young's modulus, GPa	Poisson's ratio	Density, kg⋅m ³	The angle of internal friction, $^{\circ}$	Cohesive, MPa
Casing	210.0	0.30	7850.0	_	_
Cement	10.0	0.17	1800.0	27.0	8.0
Rock	32.0	0.20	2500.0	38.0	12.5

Table 3Input parameters for numerical simulation of the hydraulic fracturing-induced fault activation process.

Parameters	Value	Unit	Parameters	Value	Unit
Young's modulus	32.0	GPa	Fault initial aperture	0.1	mm
Poisson's ratio	0.20	_	Fault tensile strength	0	MPa
Matrix cohesion	3.7	MPa	Maximum horizontal principal stress	100.0	MPa
Matrix internal friction angle	40.0	•	Minimum horizontal principal stress	85.0	MPa
Fault cohesive	1.5	MPa	Vertical stress	92.0	MPa/m
Friction angle within the fault	33.0	0	Pore pressure	75.0	MPa

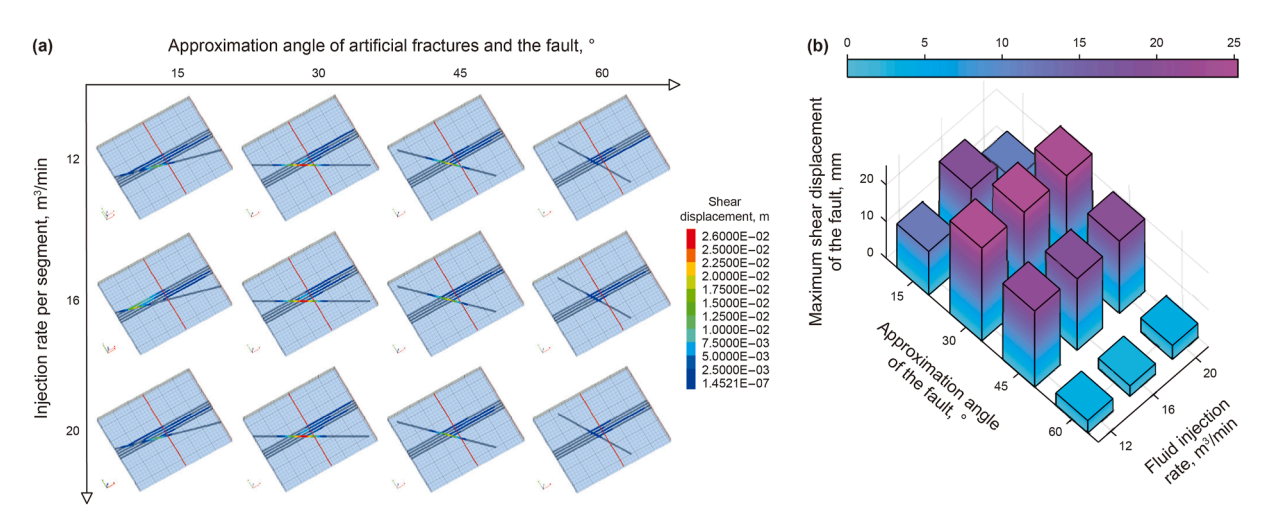


Fig. 5. Numerical simulation of hydraulic fracturing and fault activation under four clusters per segment: (a) the lengths of activated faults under different injection rates and approximation angles of the faults; (b) the fault slip distance under different injection rates and approximation angles of the faults.

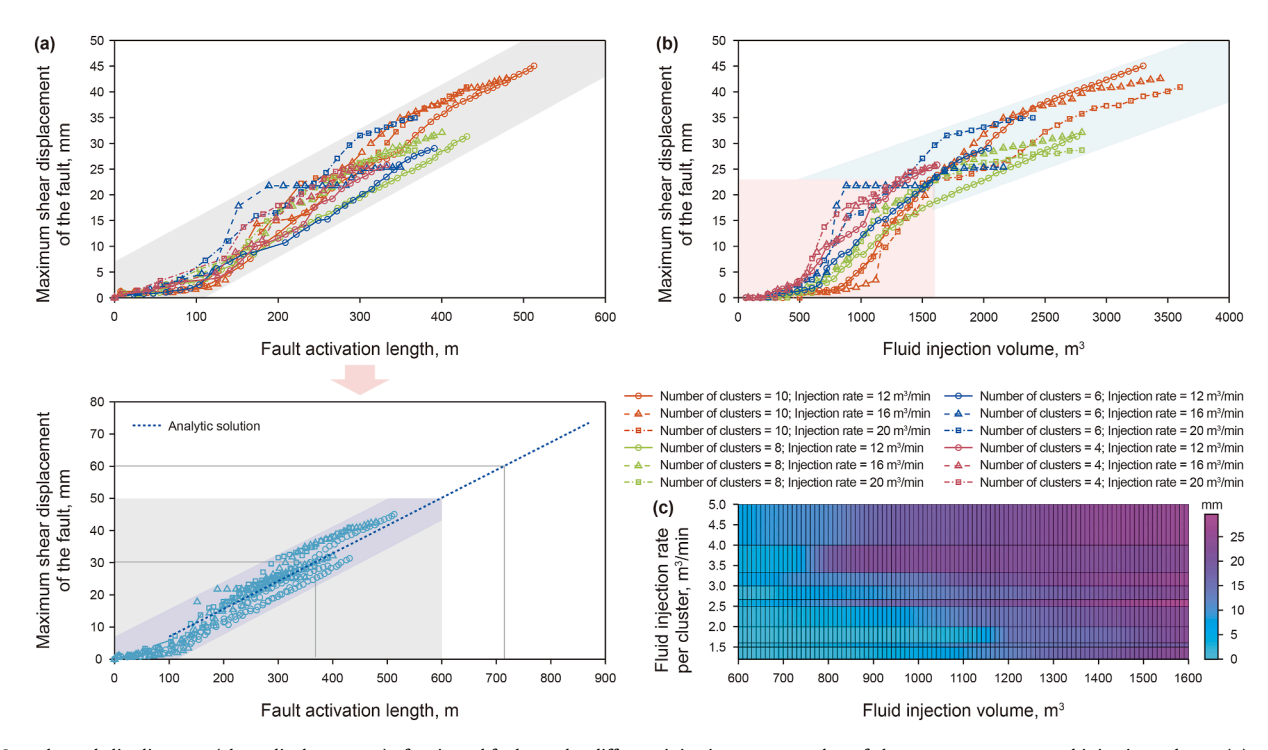


Fig. 6. Lengths and slip distances (shear displacements) of activated faults under different injection rates, number of clusters per segment, and injection volume: (a) maximum shear displacement of faults at different fault activation lengths; (b) maximum shear displacement of the fault at different fluid injection volumes; (c) maximum shear displacement of the fault at different fluid injection volumes and injection rates.

which means that the casing deformation will also be less than 36 mm. However, in the deep shale gas fracturing process in Southwest China, several wells have casing deformations of even more than 60 mm. This is possible because the length of the activation fault is underestimated. While analyzing the field fracturing data, we found that frac hits (Hou et al., 2022) caused by

fault activation occurred frequently. This means that it is possible that multiple fracturing of multiple wells will lead to a wider-scale activation of the fault.

To study the cumulative process of fault activation and fault slip during well-factory fracturing, we implemented a numerical model containing three horizontal wells and a fault is established. Each well is fractured in the high-risk section (fracturing segment close to the fault), and Well 1, Well 2, and Well 3 are fractured one by one. The fault activation process is simulated under different fluid injection volumes, as shown in Fig. 7. Comparing the maximum shear displacement of the faults at different injection rates, we found that the maximum shear displacement of the faults at the end of the fracturing of Well 1 shows an approximately linear increase with the increase of the fluid injection rate, which is consistent with the conclusion in Section 3.2. It is noteworthy that Well 2 and Well 3 show an exponential rise in fault slip distance when fracturing is completed. According to the results of numerical simulations, the reason for this phenomenon is that faults are activated several times and communicated, as shown in Fig. 7(a) and (b). Frac hits will occur when the injection volume per segment exceeds 1000 m³ (Fig. 7(b)). When the injection volume is 1200 m³, the maximum shear displacement has exceeded 40 mm (Fig. 7(c)), which means that there is an extremely high probability that serious casing deformation will occur. In the simulation of single-well fracturing, when the injection volume is 3600 m³, the maximum fault slip distance still does not exceed 50 mm (see Fig. 6). In the well-factory fracturing mode, the maximum fault slip distance even exceeded 80 mm when the injection volume per segment is 1800 m^3 (Fig. 7(d)). This proves that our previous speculation is correct. When the well field fracturing technique is used, the injection volume per segment is usually about 2000 m³ in Southwest China's shale reservoirs. Combined with the results of numerical simulation, we suggest that in the high-risk fracturing stages, the injection volume per segment should be no more than 800 m³ to reduce the geological risk (Frac hits and casing deformation) as much as possible. If only a maximum shear displacement of less than 30 mm is expected, the injection volume per segment should be no more than 1000 m^3 .

3.4. Field application studies

In laboratory experiments and numerical simulations, it is extremely difficult to completely realize the in-situ conditions of the reservoir. Especially in numerical modeling, a moderate model simplification is usually essential. Therefore, to validate the conclusions of the previous studies, we chose to carry out some field application studies. We carry out some field application studies of fracturing in a deep shale gas reservoir (LZ block). The fracturing process is monitored by surface microseismic, and the monitoring service is provided by BGP (Bureau of Geophysical Prospecting INC). First, we would like to verify whether the hydraulic fracture can cross the faults. During design, fracturing segments are categorized according to the risk of casing deformation. If a fracturing segment intersects with a fault, then it is defined as a high-risk segment. Fracturing segments adjacent to high-risk segments are defined as medium-risk segments. The other segments are lowrisk segments, which means that common fracturing design parameters can be used, and the risk of fault activation and casing deformation is minimal. The distribution of faults can be obtained from curvature bodies interpreted from 3D seismic data, and the curvature calculation service is provided by Schlumberger. In the design of the well package on the L1 platform, the injection volume per segment is 2000 m³, and the injection rate is 16 m³/min. In the low-risk segment, there are 6-8 clusters per segment. In the high-risk and medium-risk sections, there are 4 clusters per segment. Reservoir curvature and microseismic monitoring results are shown in Fig. 8(a). We found that it is difficult to achieve hydraulic fracture across the fault by reducing the number of clusters. Moreover, the large amount of fluid entering the fault may increase the risk of fault activation and casing deformation. This justifies the conclusions of Section 3.2 and means that the activation of faults seems to be unavoidable in the process of hydraulic fracturing. To reduce the risk of fault activation, we tried to minimize the injection volume of high-risk segments in the fracturing design of the well group on the L2 platform. The injection volume is 1800 m³ in the low-risk segments and 1200 m³ in the high-risk and medium-risk segments. On the L2 platform, there is a large-scale fault that crosses multiple wells, and the

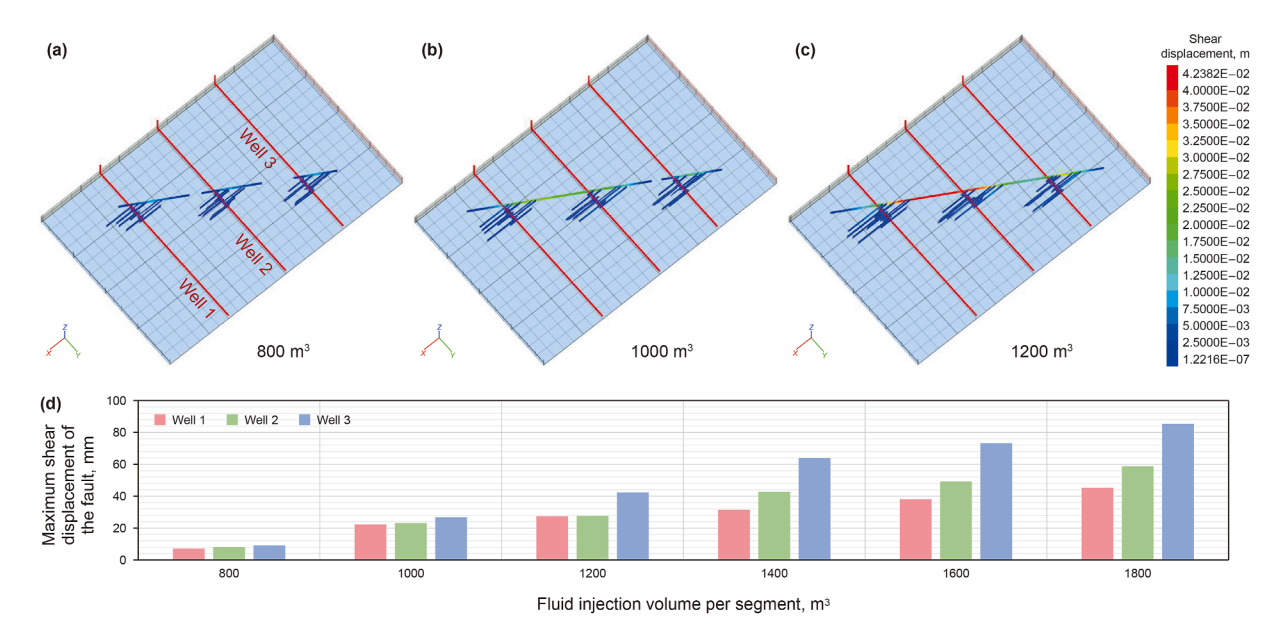


Fig. 7. Numerical simulation of hydraulic fracturing and fault activation in the well-factory fracturing model under different injection volumes: (**a**) distribution of activated faults with fluid injection volume is 800 m³; (**b**) distribution of activated faults with fluid injection volume is 1000 m³; (**c**) distribution of activated faults with fluid injection volume is 1200 m³; (**d**) maximum shear displacement of activated faults at different fluid injection volumes.

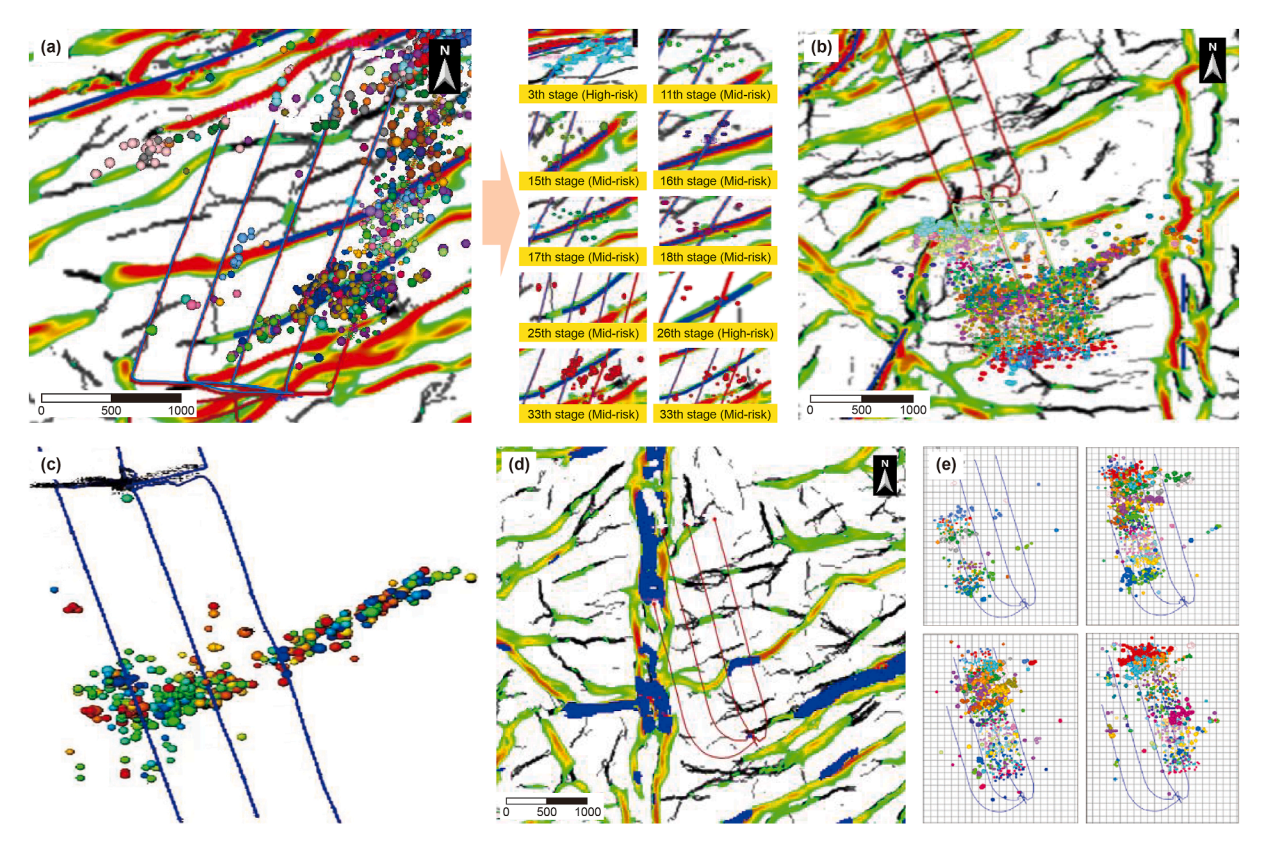


Fig. 8. Reservoir curvature distribution and microseismic monitoring results: (a) curvature and microseismic event distribution of the L1 platform; (b) curvature and microseismic event distribution of the L2 platform; (c) distribution of microseismic events near faults of the L2 platform; (d) curvature distribution of the L3 platform; (e) distribution of microseismic events for each well of the L3 platform.

approximation angle is about 30° (Fig. 8(b)). During hydraulic fracturing, an extremely severe casing deformation occurred on the right side of the well, causing subsequent fracturing to be interrupted. The distribution of microseismic events near the fault is shown in Fig. 8(c). We observed that hydraulic fracturing of multiple wells leads to the activation of the fault at several different locations. When these activation faults are connected, the scale of fault activation increases exponentially and induces severe casing deformation. This means that the injection volume in the high-risk segments should be further reduced under the wellfactory fracturing model. This is also consistent with the conclusions in Section 3.3. Based on the conclusions obtained in Sections 3.2 and 3.3, we optimized the fracturing design of the L3 platform. In the L3 platform, there is a large-scale fault with an approximation angle of less than 15°, as shown in Fig. 8(d). For a high-risk fault with an approach angle of 30°, the maximum injection volume in well-factory fracturing mode is 800 m³. Considering that the slip distance of the fault with an approximation angle of 15° is estimated to be 55.71% of the slip distance of the fault with an approximation angle of 30°, the maximum injection volume in the risk segment of the L3 platform is 1436 m³. Finally, during the fracturing process on the L3 platform, the injection volume in the low-risk segment is 1800 to 2000 m³ per segment, with 6 clusters per segment. In the high-risk segment, the injection volume per segment is 1400 to 1500 m³, with 10–11 clusters per segment. The results of microseismic monitoring of the fracturing process are shown in Fig. 8(e), which indicates that there is no serious casing deformation during the fracturing process, and all the fracturing is completed successfully.

4. Conclusions

Various methods have been used to study hydraulic fracturing-induced fault activation and casing deformation. A large amount of field data on fracturing is counted, and the main influencing factors are analyzed based on statistical methods. Combined with physical experiments and numerical simulations, the fault activation law during fracturing has been studied, and the optimization method of hydraulic fracturing parameters is proposed. The field application study verifies the correctness of the theoretical results, and the conclusions obtained are as follows:

- (1) The degree of casing deformation and fault slip are linearly correlated. The main factors of hydraulic fracturing-induced fault slip are (from strong to weak) parameters related to fluid injection volume, parameters related to segments and clusters, and parameters related to injection rate. If the fracturing fluid enters the fault, the cohesion and internal friction angle of the weak structural surface of the shale will be reduced.
- (2) Using common hydraulic fracturing techniques, it is very difficult for hydraulic fractures to cross faults. Even if a few hydraulic fractures can cross the fault with a fault approximation angle greater than 60°, the fractures cannot continue to propagate. This means that large amounts of fluid can be injected into faults and increase the risk of fault activation.
- (3) The risk of hydraulic fracturing-induced fault activation is the greatest when the approximation angle of the fault is close to the angle of internal friction. The number of clusters

per segment and the injection rate are negatively correlated with the fault slip distance. Reducing the fluid injection volume can mitigate the fault slip distance. Therefore, low injection rates, low fluid volumes, and more clusters per segment are recommended for fracturing in high-risk segments.

- (4) When only one well needs to be fractured, the fault slip distance increases linearly with increasing injection volume. However, the scale of fault activation will be larger when fracturing in a well field. The maximum fault slip distance increases exponentially with increasing injection volume. In situations with extremely high risk, the injection volume should preferably not exceed 800 m³.
- (5) Mapping the faults in advance using three dimensional seismic surveys (where the curvature attribute is calculated from) is absolutely essential to determine if a shale gas well is located in a high-risk area for casing deformation or not.

CRediT authorship contribution statement

Yu-Ting He: Writing – original draft, Visualization, Methodology, Investigation. **Yin-Tong Guo:** Resources, Project administration, Investigation. **Yun Jiang:** Validation, Resources, Funding acquisition, Data curation. **Xin Chang:** Writing – review & editing, Visualization, Investigation. **Yu-Xiang Jing:** Writing – review & editing, Supervision, Investigation. **Ming-Nan Xu:** Writing – review & editing, Visualization, Project administration. **Chun-He Yang:** Resources, Project administration, Conceptualization.

Declaration of competing interest

We declare that we have no financial and personal relationships with other people or organizations that can inappropriately influence our work, there is no professional or other personal interest of any nature or kind in any product, service and/or company that could be construed as influencing the position presented in, or the review of, the manuscript entitled, "Hydraulic fracturing induced casing deformation and fault activation: from single-well fracturing to well-factory fracturing."

Acknowledgment

This work was financially supported by the National Natural Science Foundation of China (U24B2035 and 52304070), Post-doctoral Fellowship Program of CPSF (GZC20241889 and 2024M753456), and Natural Science Foundation of Hubei Province of China (2024AFD374).

Appendix A. Supplementary data

Supplementary data to this article can be found online at https://doi.org/10.1016/j.petsci.2025.07.014.

References

- Bao, X., Eaton, D.W., 2016. Fault activation by hydraulic fracturing in western Canada. Science 354 (6318), 1406–1409. https://doi.org/10.1126/science. aag258.
- Bhattacharya, P., Viesca, R.C., 2019. Fluid-induced aseismic fault slip outpaces pore-fluid migration. Science 364 (6439), 464–468. https://doi.org/10.1126/science.aaw735.
- Chang, X., Wang, X., Yang, C., et al., 2024. Experimental investigation on mode I fracture characteristics of Longmaxi Formation shale after cyclic thermal shock and high-temperature acid etching treatments. Eng. Fract. Mech. 295, 109762. https://doi.org/10.1016/j.engfracmech.2023.109762.

Chen, Y., Li, J., Lu, H., et al., 2020. Tradeoffs in water and carbon footprints of shale gas, natural gas, and coal in China. Fuel 263, 116778. https://doi.org/10.1016/j.fuel.2019.116778.

- Das, I., Zoback, M.D., 2011. Long-period, long-duration seismic events during hydraulic fracture stimulation of a shale gas reservoir. Lead. Edge 30 (7), 778–786. https://doi.org/10.1002/2017GL073582.
- Dou, Z., Gao, T., Zhao, Z., et al., 2020. The role of water lubrication in critical state fault slip. Eng. Geol. 271, 105606. https://doi.org/10.1016/j.enggeo.2020.
- Ellsworth, W.L., 2013. Injection-induced earthquakes. science 341 (6142), 1225942. https://doi.org/10.1126/science.1225942.
- Frash, L.P., Meng, M., Li, W., et al., 2025. Exploring the physical limits of hydraulic fracture caging to forecast its feasibility for geothermal power generation. Renew. Energy 241, 122364. https://doi.org/10.1016/j.renene.2025.122364.
- Fu, H., Huang, L., Hou, B., et al., 2024. Experimental and numerical investigation on interaction mechanism between hydraulic fracture and natural fracture. Rock Mech. Rock Eng. 57, 10571–10582. https://doi.org/10.1007/s00603-024-04101-3
- He, Y., Chen, Z., Li, X., et al., 2023. Self-supporting conductivity in shallow and ultra shallow shale reservoirs: under hydraulic, CO₂ and Sc-CO₂ fracturing. Geoenergy Sci. Eng. 223, 211557. https://doi.org/10.1016/j.geoen.2023.211557.
- He, Y., Guo, Y., Bi, Z., et al., 2025. Study of field-scale carbon dioxide fracturing in hot dry rock reservoir based on a new 3D-THM coupled discrete block model. Geoenergy Sci. Eng. 247, 213675. https://doi.org/10.1016/j.geoen.2025.213675.
- He, Y., Guo, Y., Yang, Z., et al., 2024. Integrated study of hydraulic/CO₂ fracturing and production coupled with a THM-D process in ultra-shallow shale reservoirs. Nat. Gas. Ind. B 11 (5), 581–602. https://doi.org/10.1016/j.ngib.2024. 09 001
- Hou, B., Zhang, Q., Liu, X., et al., 2022. Integration analysis of 3D fractures network reconstruction and frac hits response in shale wells. Energy 260, 124906. https://doi.org/10.1016/j.energy.2022.124906.
- Hui, G., Chen, S., Gu, F., et al., 2021. Influence of hydrological communication between basement-rooted faults and hydraulic fractures on induced seismicity: a case study. J. Petrol. Sci. Eng. 206, 109040. https://doi.org/10.1016/j.petrol.2021.109040.
- Lei, Q., Zhang, J., Zhu, X., et al., 2024. Experimental study on shear deformation mechanism and mitigation in shale gas casing. Eng. Fail. Anal. 159, 108056. https://doi.org/10.1016/j.engfailanal.2024.108056.
- Li, J., Xu, J., Zhang, H., et al., 2023. High seismic velocity structures control moderate to strong induced earthquake behaviors by shale gas development. Commun. Earth Environ. 4 (1), 188. https://doi.org/10.1038/s43247-023-00854-x
- Li, X., Lu, S., Zhao, S., et al., 2024. Gas-in-place content and occurrence state of deep shale gas in the Luzhou area, Sichuan Basin, China. Mar. Petrol. Geol. 160, 106662. https://doi.org/10.1016/j.marpetgeo.2023.106662.
- Liu, K., Taleghani, A.D., Gao, D., 2019. Calculation of hydraulic fracture induced stress and corresponding fault slippage in shale formation. Fuel 254, 115525. https://doi.org/10.1016/j.fuel.2019.05.108.
- Madenova, Y., Frash, L.P., Li, W., et al., 2025. Fracture caging in a lab fault to prevent seismic rupture during fluid injection. Geothermics 126, 0103206. https://doi.org/10.1016/j.geothermics.2024.103206.
- Meng, L., McGarr, A., Zhou, L., et al., 2019. An investigation of seismicity induced by hydraulic fracturing in the Sichuan Basin of China based on data from a temporary seismic network. Bull. Seismol. Soc. Am. 109 (1), 348–357. https:// doi.org/10.1785/0120180310.
- Moein, M.J.A., Langenbruch, C., Schultz, R., et al., 2023. The physical mechanisms of induced earthquakes. Nat. Rev. Earth Environ. 4 (12), 847–863. https://doi.org/ 10.1038/s43017-023-00497-8.
- Papantonis, D., Stavrakas, V., Tzani, D., et al., 2025. Towards decarbonisation or lock-in to natural gas? A bottom-up modelling analysis of the energy transition ambiguity in the residential sector by 2050. Energy Convers. Manag. 324, 119235. https://doi.org/10.1016/j.enconman.2024.119235.
- Rutqvist, J., Rinaldi, A.P., Cappa, F., et al., 2013. Modeling of fault reactivation and induced seismicity during hydraulic fracturing of shale-gas reservoirs. J. Petrol. Sci. Eng. 107, 31–44. https://doi.org/10.1016/j.petrol.2013.04.023.
- Schultz, R., Atkinson, G., Eaton, D.W., et al., 2018. Hydraulic fracturing volume is associated with induced earthquake productivity in the Duvernay play. Science 359 (6373), 304–308. https://doi.org/10.1126/science.aao0159.
- Schultz, R., Beroza, G.C., Ellsworth, W.L., 2021. A risk-based approach for managing hydraulic fracturing-induced seismicity. Science 372 (6541), 504–507. https:// doi.org/10.1126/science.abg5451.
- Schultz, R., Skoumal, R.J., Brudzinski, M.R., et al., 2020. Hydraulic fracturing-induced seismicity. Rev. Geophys. 58 (3), e2019RG000695. https://doi.org/10.1029/2019RG000695.
- Shen, C., Wu, J., Zeng, B., et al., 2024. Measures and results of prevention and control on casing deformation and frac-hit in deep shale gas wells in Southern Sichuan Basin. Nat. Gas. Ind. B 11 (3), 262–273. https://doi.org/10.1016/j. ngib.2024.05.006.
- Sun, Z.H., Che, M.G., Zhu, L.H., et al., 2024. Implications for fault reactivation and seismicity induced by hydraulic fracturing. Pet. Sci. 21 (2), 1081–1098. https:// doi.org/10.1016/j.petsci.2023.11.022.
- Tan, Y., Hu, J., Zhang, H., et al., 2020. Hydraulic fracturing induced seismicity in the southern Sichuan Basin due to fluid diffusion inferred from seismic and

- injection data analysis. Geophys. Res. Lett. 47 (4), e2019GL084885. https://doi.org/10.1029/2019GL084885.
- Xie, Q., Li, C., Chen, G., et al., 2025. Joint application of seismic multi-attribute in multi-scale fracture prediction of LZ shale gas block, Sichuan Basin, China. Acta Geophys. 73, 2423–2442. https://doi.org/10.1007/s11600-024-01516-y.
- Xu, W., Zhao, J., Rahman, S.S., et al., 2019. A comprehensive model of a hydraulic fracture interacting with a natural fracture: analytical and numerical solution. Rock Mech. Rock Eng. 52, 1095–1113. https://doi.org/10.1007/s00603-018-1608-9.
- Yan, Y., Cai, M., Ma, W.H., et al., 2024. Research on casing deformation prevention technology based on cementing slurry system optimization. Pet. Sci. 21 (2), 1231–1240. https://doi.org/10.1016/j.petsci.2023.10.018.
 Zelenin, E., Bachmanov, D., Garipova, S., et al., 2022. The database of the active
- Zelenin, E., Bachmanov, D., Garipova, S., et al., 2022. The database of the active faults of Eurasia (AFEAD): ontology and design behind the continental-scale dataset. Earth Syst. Sci. Data Discuss. 14 (10), 4489–4503. https://doi.org/ 10.5194/essd-14-4489-2022.
- Zhang, F., Jiang, Z., Chen, Z., et al., 2020. Hydraulic fracturing induced fault slip and casing shear in Sichuan Basin: a multi-scale numerical investigation. J. Petrol. Sci. Eng. 195, 107797. https://doi.org/10.1016/j.petrol.2020.107797.

- Zhang, X., Li, J., Zhang, H., et al., 2021. Analysis of casing deformation failure mechanism based on fault slip. Eng. Fail. Anal. 127, 105430. https://doi.org/10.1016/j.engfailanal.2021.105430.
- Zhao, C., Li, J., Zaman, M., et al., 2021. Investigation of casing deformation characteristics under cycling loads and the effect on casing strength based on full-scale equipment. J. Petrol. Sci. Eng. 205, 108973. https://doi.org/10.1016/j.petrol.2021.108973.
- Zheng, Y., He, R., Huang, L., et al., 2022. Exploring the effect of engineering parameters on the penetration of hydraulic fractures through bedding planes in different propagation regimes. Comput. Geotech. 146, 104736. https://doi.org/10.1016/i.compgeo.2022.104736.
- Zhao, G., Guo, Y., Yang, C., et al., 2023. Anisotropic mechanical behavior of ultradeep shale under high in-situ stress, a case study in the Luzhou block of the southern Sichuan Basin, China. Int. J. Rock Mech. Min. Sci. 170, 105536. https:// doi.org/10.1016/j.ijrmms.2023.105536.